CONDITIONAL SIMULATION OF SPATIALLY CORRELATED EARTHQUAKE GROUND MOTION

By Erik H. Vanmarcke,[1] Ernesto Heredia-Zavoni,[2] and Gordon A. Fenton[3]

ABSTRACT: Methodology is presented for simulating properly correlated earthquake ground motions at an arbitrary set of closely spaced points, compatible with known or prescribed motions at other locations. The input consists of the spectral density function and frequency-dependent spatial correlation function in several nonoverlapping ground-motion segments. Linear-prediction estimators are used to generate a set of statistically independent, frequency-specific, spatial random processes, based on which ground motions are composed by means of a fast-Fourier-transform algorithm. The method's advantage over existing linear-estimation techniques, known as kriging, is that it correctly reproduces the specified space-time correlation structure of the ground motion. Examples are given to illustrate the features of the simulation methodology; in particular, response spectra and dynamic response ratios are compared for recorded and simulated motions at the site of the SMART 1 strong-motion accelerograph array.

INTRODUCTION

Although simulating spatially correlated earthquake ground motion has become straightforward in principle, provided the space-time correlation structure of the ground motion is known or prescribed, it is only recently that the problem of conditional simulation has been addressed (Vanmarcke and Fenton 1989, 1991). In conditional simulation, motions have been recorded, or specified for design purposes, at a number of closely spaced points, and the aim is to generate compatible accelerograms at nearby locations where motions are not available. For instance, ground motions may be given at one or more points at the site of a multisupport structure; to provide input into structural response analysis, it is necessary to "predict" the ground motions at the location of the supports. In another important application, one may seek to predict the ground motion at the site of a damaged or collapsed structure after an earthquake, based on recorded ground motions nearby. Fenton and Vanmarcke (1989) proposed the use of linear-estimation techniques called kriging developed for regionalized random variables in geostatistics (Matheron 1967), for the conditional simulation of stationary segments of earthquake ground motion, later extending the methodology to account for time-varying ground-motion intensity and frequency content. In this paper, an improved methodology based on linear-prediction theory is presented; its advantage is that the covariance structure of the simulated process correctly reproduces the theoretical covariance structure under all circumstances expected to be encountered in engineering applications. In the context of modeling local fields of earthquake ground motion, this is a significant improvement over the kriging techniques that

[1]Prof., Dept. of Civ. Engrg., Princeton Univ., Princeton, NJ 08540.
[2]Grad. Student, Dept. of Civil Engrg., Princeton University, Princeton, NJ.
[3]Assistant Professor, Dept. of Applied Mathematics, Tech. Univ. of Nova Scotia, Halifax, Nova Scotia, Canada.

Note. Discussion open until April 1, 1994. To extend the closing date one month, a written request must be filed with the ASCE Manager of Journals. The manuscript for this paper was submitted for review and possible publication on July 6, 1992. This paper is part of the ***Journal of Engineering Mechanics***, Vol. 119, No. 11, November, 1993. ©ASCE, ISSN 0733-9399/93/0011-2333/$1.00 + $.15 per page. Paper No. 4400.

poorly preserve the covariance structure of the ground motion, and in particular, its spectral density function and amplitudes at locations relatively far from the points where motions are prescribed (Heredia-Zavoni 1993).

The simulation of phase-aligned earthquake ground motion using fast-Fourier-transform (FFT) techniques is first examined: phase alignment refers to the extraction of time delays associated with wave travel along the path of seismic wave propagation. We then analyze the kriging and linear-prediction estimators for the case of a scalar or component spatial random process, assuming that a set of points the process has been observed, with interest focusing on how to predict values of the process at a set of target points. Next we discuss the use of kriging and linear-prediction estimators in a conditional simulation algorithm, and examine the conditions under which the simulated process reproduces the covariance structure of the true process. An improved methodology for the conditional simulation of a phase-aligned earthquake ground motion process, modeled as the sum of a series of uncorrelated frequency-specific spatial processes, is then presented. Finally, some examples are presented to illustrate the features, capabilities, and uses of the simulation methodology. Results mimicking data from the Taiwan Strong Motion Array (SMART 1) are also given and serve to compare simulated and recorded ground motions.

GROUND-MOTION SIMULATION

Assume that a segment of the ground motion at a point x_i can be represented by a nonergodic, zero-mean, homogeneous, mean-square continuous space time process $Z_i(t)$. The process $Z_i(t)$ can be expressed as a sum of independent frequency-specific spatial processes in consecutive constant-size frequency intervals, $\Delta\omega$, as follows.

$$Z_i(t) = \sum_{k=1}^{K} [A_{ik} \cos(\omega_k t) + B_{ik} \sin(\omega_k t)] \quad \ldots\ldots\ldots\ldots\ldots\ldots\ldots\ldots (1)$$

where the coefficients A_{ik} and B_{ik} = zero-mean random variables. For a discrete-time process, $Z_i(t_j)$, defined at times $t_j = (j - 1)\Delta t$, $j = 1, 2, \ldots, K$, the coefficients A_{ik} and B_{ik} are related to $Z_i(t_j)$ through the discrete direct fourier transform

$$A_{ik} = \frac{1}{K} \sum_{j=1}^{K} Z_i(t_j) \cos\left[\frac{2\pi(k-1)(j-1)}{K}\right] \quad \ldots\ldots\ldots\ldots\ldots\ldots (2a)$$

$$B_{ik} = \frac{1}{K} \sum_{j=1}^{K} Z_i(t_j) \sin\left[\frac{2\pi(k-1)(j-1)}{K}\right] \quad \ldots\ldots\ldots\ldots\ldots\ldots (2b)$$

where $\Delta t = t_f/(K - 1)$; $\omega_k = (k - 1)\Delta\omega$; $\Delta\omega = 2\pi/(t_f + \Delta t)$; $k = 1, 2, \ldots, K$; and t_f = the length of the process. The basic concepts pertinent to simulation using Fourier transforms can be found in Priestley (1981). The following symmetry conditions about the Nyquist frequency, $\omega_{(1+K)/2} = \pi/\Delta t$, apply to the Fourier coefficients A_{ik} and B_{ik}, when the process $Z_i(t_j)$ is real.

$$A_{ik} = A_{i(K-k+2)}, \quad B_{ik} = -B_{i(K-k+2)} \qquad \text{for } k = 2, 3, \ldots, \frac{1+K}{2} \quad \ldots (3)$$

Heredia-Zavoni (1993) has shown that by using (2), the covariance, $C_{ij}(\omega_k) = EA_{ik}A_{jk}$, between coefficients at points x_i and x_j can be written as follows.

$$C_{ij}(\omega_k) = \frac{1}{2}\rho\omega_k(\mathbf{r}_{ij})G(\omega_k)\Phi\omega, \qquad \text{for } k = 1 \quad \ldots\ldots\ldots\ldots\ldots\ldots (4a)$$

$$C_{ij}(\omega_k) = \frac{1}{4}\{\rho_{\omega k}(\mathbf{r}_{ij})G(\omega_k) + \rho_{\omega K-k+2}(\mathbf{r}_{ij})G(\omega_{K-k+2})\}\Delta\omega,$$

$$\text{for } k = 2, \ldots, \frac{K}{2} \quad \ldots\ldots\ldots\ldots\ldots\ldots\ldots\ldots\ldots\ldots\ldots\ldots\ldots\ldots (4b)$$

$$C_{ij}(\omega_k) = \rho_{\omega k}(\mathbf{r}_{ij})G(\omega_k)\Delta\omega, \qquad \text{for } k = \frac{1+K}{2} \quad \ldots\ldots\ldots\ldots\ldots\ldots (4c)$$

where $\mathbf{r}_{ij} = x_i - x_j$ = the relative position vector; $G(\omega)$ = the one-sided "point" spectral-density function; and $\rho_{\omega k}(\mathbf{r}_{ij})$ = the frequency-dependent spatial correlation function. $EA_{ik}A_{jk} = EB_{ik}B_{jk} = C_{ij}(\omega_k)$ for $k = 2, \ldots, K/2$.

The spatially correlated ground motions are obtained by generating sets of Fourier coefficients A_{ik} and B_{jk}, for each frequency ω_k, $k = 1, 2, \ldots, (1 + K)/2$ [the remainder obtained using the symmetry conditions in (3)], then using an FFT algorithm to perform the inverse discrete transform. The technique of summing frequency-specific spatial processes to simulate local fields of ground motion makes efficient use of available information about earthquake ground motion, in the form of the spectral density function and the frequency-dependent spatial correlation function in different segments, and of the mutual statistical independence of component spatial fields (Vanmarcke 1983). The focus in the next few sections is on the modeling of individual, frequency-specific contributions to the local field of phase-aligned ground motions.

KRIGING ESTIMATION

Consider a set of n recording points x_α [$\alpha = (1, 2, \ldots, n)$], at which the values of a spatial random process $Z(x)$ is observed, measured, or specified [$Z(x_\alpha)$], and a set of m target points x_β [$\beta = (n + 1, n + 2, \ldots, n + m)$], at which the process $Z(x_\beta)$ is unknown, to be estimated using kriging (Journel and Huijbregts 1978; Matheron 1967). The kriging estimator of the value of the process at a target point x_β, denoted here by $Z^*_K(x_\beta)$, is expressed as a linear combination of the observed values at the recording points

$$Z^*_K(x_\beta) = \boldsymbol{\lambda}^T_{\beta\alpha}\mathbf{Z}(x_\alpha) \quad \ldots\ldots\ldots\ldots\ldots\ldots\ldots\ldots\ldots\ldots\ldots\ldots\ldots\ldots (5)$$

where $\mathbf{Z}^T(x_\alpha) = [Z(x_1), Z(x_2), \ldots, Z(x_n)]$ = the set of known values; the elements in the vector $\boldsymbol{\lambda}^T_{\beta\alpha} = (\lambda_{\beta 1}, \lambda_{\beta 2}, \ldots, \lambda_{\beta n})$ are the so-called kriging weights; and the superscript T denotes matrix transposition. The vector of kriging weights $\boldsymbol{\lambda}_{\beta\alpha}$ is determined so that the estimator is unbiased and the mean square error (MSE) minimized. Suppose that the mean of the process is constant but known, $EZ(x) = m_o$. The condition imposed on the kriging weights to ensure the lack of bias of the estimator, $EZ^*_K(x_\beta) = m_o$, is

$$\boldsymbol{\lambda}^T_{\beta\alpha}\mathbf{J} = 1, \qquad \beta = n + 1, n + 2, \ldots, n + m \quad \ldots\ldots\ldots\ldots\ldots\ldots (6)$$

where $\mathbf{J}$ = an n-dimensional vector of ones. The MSE can be written as follows:

$$E[Z_K^*(x_\beta) - Z(x_\beta)]^2 = C_{\beta\beta} - 2\boldsymbol{\lambda}_{\beta\alpha}^T \mathbf{C}_{\alpha\beta} + \boldsymbol{\lambda}_{\beta\alpha}^T \mathbf{C}_{\alpha\alpha} \boldsymbol{\lambda}_{\beta\alpha} \quad \ldots\ldots\ldots\ldots (7)$$

where $C_{\beta\beta}$ = var $Z(x\beta)$; $\mathbf{C}_{\alpha\beta}$ = cov$[Z(x_\alpha), Z(x_\beta)]$; and $\mathbf{C}_{\alpha\alpha}$ = cov $Z(x_\alpha)$. Thus, obtaining the kriging weights involves minimizing the expression in (7) subject to the constraint in (6). Using a Lagrange multiplier, μ, a system of linear equations is obtained.

$$\boldsymbol{\lambda}_{\beta\alpha}^T \mathbf{C}_{\alpha\alpha} = \mu \mathbf{J}^T + \mathbf{C}_{\alpha\beta}^T \quad \ldots\ldots\ldots\ldots (8a)$$

$$\boldsymbol{\lambda}_{\beta\alpha}^T \mathbf{J} = 1 \quad \ldots\ldots\ldots\ldots (8b)$$

which has a unique solution if and only if the covariance matrix $\mathbf{C}_{\alpha\alpha}$ is positive definite. Solving the system of equations for the vector of kriging weights yields

$$\boldsymbol{\lambda}_{\beta\alpha} = \mathbf{C}_{\alpha\alpha}^{-1} \mathbf{C}_{\alpha\beta} + \frac{1 - \mathbf{J}^T \mathbf{C}_{\alpha\alpha}^{-1} \mathbf{C}_{\alpha\beta}}{\mathbf{J}^T \mathbf{C}_{\alpha\alpha}^{-1} \mathbf{J}} \mathbf{C}_{\alpha\alpha}^{-1} \mathbf{J} \quad \ldots\ldots\ldots\ldots (9)$$

It then follows from (5) that $Z_K^*(x_\beta)$ is given by

$$Z_K^*(x_\beta) = \mathbf{C}_{\alpha\beta}^T \mathbf{C}_{\alpha\alpha}^{-1} Z(x_\alpha) + \frac{1 - \mathbf{J}^T \mathbf{C}_{\alpha\alpha}^{-1} \mathbf{C}_{\alpha\beta}}{\mathbf{J}^T \mathbf{C}_{\alpha\alpha}^{-1} \mathbf{J}} \mathbf{J}^T \mathbf{C}_{\alpha\alpha}^{-1} \mathbf{Z}(x_\alpha) \quad \ldots\ldots\ldots\ldots (10)$$

$$Z_K^*(x_\beta) = \left(\mathbf{C}_{\alpha\beta}^T \mathbf{C}_{\alpha\alpha}^{-1} - \frac{\mathbf{J}^T \mathbf{C}_{\alpha\alpha}^{-1} \mathbf{C}_{\alpha\beta}}{\mathbf{J}^T \mathbf{C}_{\alpha\alpha}^{-1} \mathbf{J}} \mathbf{J}^T \mathbf{C}_{\alpha\alpha}^{-1} \right) \mathbf{Z}(x_\alpha) + \frac{\mathbf{J}^T \mathbf{C}_{\alpha\alpha}^{-1} \mathbf{Z}(x_\alpha)}{\mathbf{J}^T \mathbf{C}_{\alpha\alpha}^{-1} \mathbf{J}} \quad \ldots\ldots (11)$$

The second term in (11) is the part of the estimator that does not depend on the covariance matrix of the process between target and recording points; this term is the best linear unbiased estimator (BLUE) of the unknown mean, $\hat{m}_o$ (Watson 1970)

$$\hat{m}_o = \frac{\mathbf{J}^T \mathbf{C}_{\alpha\alpha}^{-1} \mathbf{Z}(x_\alpha)}{\mathbf{J}^T \mathbf{C}_{\alpha\alpha}^{-1} \mathbf{J}} \quad \ldots\ldots\ldots\ldots (12)$$

allowing the kriging estimator to be expressed as

$$Z_K^*(x_\beta) = \mathbf{C}_{\alpha\beta}^T \mathbf{C}_{\alpha\alpha}^{-1} \mathbf{Z}(x_\alpha) + (1 - \mathbf{J}^T \mathbf{C}_{\alpha\alpha}^{-1} \mathbf{C}_{\alpha\beta}) \hat{m}_o \quad \ldots\ldots\ldots\ldots (13)$$

Using (11), the conditions under which the kriging estimator is equal to the BLUE of the unknown mean, $\hat{m}_o$, can be analyzed. The first term in (11) is zero when $\mathbf{C}_{\alpha\beta} = 0$; that is, when the values of the process at target and recording points are uncorrelated. Interestingly, the first term in (11) is also zero when the matrix $\mathbf{J}\mathbf{C}_{\alpha\beta}^T$ is symmetric, i.e., $\mathbf{J}\mathbf{C}_{\alpha\beta}^T = \mathbf{C}_{\alpha\beta}\mathbf{J}^T$, which can be seen by rewriting it as follows.

$$\left(\mathbf{C}_{\alpha\beta}^T \mathbf{C}_{\alpha\alpha}^{-1} - \frac{\mathbf{J}^T \mathbf{C}_{\alpha\alpha}^{-1} \mathbf{C}_{\alpha\beta}}{\mathbf{J}^T \mathbf{C}_{\alpha\alpha}^{-1} \mathbf{J}} \mathbf{J}^T \mathbf{C}_{\alpha\alpha}^{-1} \right) \mathbf{Z}(x_\alpha) = \frac{\mathbf{J}^T \mathbf{C}_{\alpha\alpha}^{-1}}{\mathbf{J}^T \mathbf{C}_{\alpha\alpha}^{-1} \mathbf{J}} (\mathbf{J}\mathbf{C}_{\alpha\beta}^T - \mathbf{C}_{\alpha\beta}\mathbf{J}^T) \mathbf{C}_{\alpha\alpha}^{-1} \mathbf{Z}(x_\alpha)$$
$$\ldots\ldots\ldots\ldots (14)$$

The symmetry condition is also satisfied when $\mathbf{C}_{\alpha\beta} = 0$, so that, in fact, this term is zero if and only if $\mathbf{J}\mathbf{C}_{\alpha\beta}^T$ is symmetric. Since $\mathbf{J}$ is a vector of ones, it can be shown that for any $\beta = n + 1, n + 2, \ldots, n + m$

$$\mathbf{J}\mathbf{C}_{\alpha\beta}^T = \mathbf{C}_{\alpha\beta}\mathbf{J}^T \Leftrightarrow C_{i\beta} = C_{o\beta}, \qquad \forall i,\ i = 1, 2, \ldots, n, \quad \ldots\ldots\ldots\ldots (15)$$

where $C_{i\beta} = \text{cov}[Z(x_i), Z(x_\beta)]$; and $C_{o\beta}$ = a constant. Therefore, the symmetry holds when the value of the process at any target point is correlated equally with each value at the recording points. Therefore, although different target points may have different degrees of correlation with the corresponding values at the recording points, the kirging estimator will be equal to the BLUE of the unknown mean, $\hat{m}_o$, as long as the correlations between the value of the process at each target and recording points are the same. Consider, for instance, the case in which $Z^*_K(x_\beta)$ is predicted based on observations at two recording points x_α, $\alpha = 1, 2$. For simplicity of the notation, let $Z_\alpha = Z(x_\alpha)$ and $Z^*_\beta = Z^*_K(x_\beta)$. Eq. (5) reduces to

$$Z^*_\beta = \lambda_{\beta 1} Z_1 + \lambda_{\beta 2} Z_2 \quad \ldots\ldots (16)$$

and from (9), $\lambda_{\beta 1}$ and $\lambda_{\beta 2}$ are

$$\lambda_{\beta 1} = \frac{C_{2\beta} - C_{1\beta}}{2C_{12} - C_{22} - C_{11}} + \frac{C_{12} - C_{22}}{2C_{12} - C_{22} - C_{11}} \quad \ldots\ldots (17a)$$

$$\lambda_{\beta 2} = \frac{C_{1\beta} - C_{2\beta}}{2C_{12} - C_{22} - C_{11}} + \frac{C_{12} - C_{11}}{2C_{12} - C_{22} - C_{11}} \quad \ldots\ldots (17b)$$

where $C_{ij} = \text{cov}(Z_i, Z_j)$, $i, j = 1, 2$. Suppose that Z_β is equally correlated with Z_1 and Z_2, i.e., $C_{1\beta} = C_{2\beta} = C_{o\beta}$; then

$$\lambda_{\beta 1} = \frac{C_{12} - C_{22}}{2C_{12} - C_{22} - C_{11}} \quad \ldots\ldots (18a)$$

$$\lambda_{\beta 2} = \frac{C_{12} - C_{11}}{2C_{12} - C_{22} - C_{11}} \quad \ldots\ldots (18b)$$

These weights correspond to the coefficients in (12) for the BLUE of the mean, $\hat{m}_o$, and depend only on the covariances between values of the process at recording points. Eqs. (18*a*) and (18*b*) holds for any target point x_β as long as $C_{1\beta} = C_{2\beta}$. It would be desirable to have instead an estimator that accounted for the degree of correlation among Z_β, Z_1, and Z_2 through Z_2 through $C_{o\beta}$. Notice that $\lambda_{\beta 1} = \lambda_{\beta 2} = 0.5$ in case $C_{11} = C_{22}$, and one would always predict that Z^*_β equals the average of the observations Z_1 and Z_2 for all $\beta = n + 1, n + 2, \ldots, n + m$.

MULTIVARIATE LINEAR PREDICTION

Consider, as before, a set of n recording points $x_\alpha[\alpha = (1, 2, \ldots, n)]$, at which the values of a spatial random process is observed, measured, or specified $[Z(x_\alpha)]$, and a set of m target points $x_\beta[\beta = (n + 1, n + 2, \ldots, n + m)]$, where the process to be estimated is $Z(x_\beta)$. The linear-prediction estimator, $Z^*_{LP}(x_\beta)$, is expressed as a linear combination of the values at the recording points as follows:

$$Z^*_{LP}(x_\beta) = m_\beta + \boldsymbol{\kappa}^T_{\beta\alpha}[\mathbf{Z}(x_\alpha) - \mathbf{m}_\alpha] \quad \ldots\ldots (19)$$

where $m_\beta = EZ(x_\beta)$ = the known mean of the process at the target point; $Z^T(x_\alpha)$ = the set of known values; $m_\alpha = EZ(x_\alpha)$ = the known mean vector at the recording points; and $\boldsymbol{\kappa}_{\beta\alpha}$ = a vector of coefficients. The estimator is unbiased, $EZ^*_{LP}(x_\beta) = m_\beta$, and the MSE is given by

$$E[Z^*_{LP}(x_\beta) - Z(x_\beta)]^2 = C_{\beta\beta} - 2\boldsymbol{\kappa}^T_{\beta\alpha}\mathbf{C}_{\alpha\beta} + \boldsymbol{\kappa}^T_{\beta\alpha}\mathbf{C}_{\alpha\alpha}\boldsymbol{\kappa}_{\beta\alpha} \quad \ldots\ldots (20)$$

The vector of coefficients, $\boldsymbol{\kappa}_{\beta\alpha}$, minimizing the MSE is

$$\boldsymbol{\kappa}_{\beta\alpha}^{T} = \mathbf{C}_{\alpha\beta}^{T}\mathbf{C}_{\alpha\alpha}^{-1} \quad (21)$$

Substituting (21) into (19) yields with the linear-prediction estimator of the process at a target point

$$Z_{LP}^{*}(x_{\beta}) = m_{\beta} + \mathbf{C}_{\alpha\beta}^{T}\mathbf{C}_{\alpha\alpha}^{-1}[Z(\mathbf{x}_{\alpha}) - \mathbf{m}_{\alpha}] \quad (22)$$

If $\mathbf{C}_{\alpha\beta} = 0$ then $\boldsymbol{\kappa}_{\beta\alpha} = 0$, and one predicts for $Z(\mathbf{x}_{\beta})$ its mean; only variables that are correlated with $Z(\mathbf{x}_{\beta})$ are useful in linear prediction. If the mean of the process is constant, say m_o, (22) reduces to

$$Z_{LP}^{*}(x_{\beta}) = \mathbf{C}_{\alpha\beta}^{T}\mathbf{C}_{\alpha\alpha}^{-1}\mathbf{Z}(x_{\alpha}) + (1 - \mathbf{J}^{T}\mathbf{C}_{\alpha\alpha}^{-1}\mathbf{C}_{\alpha\beta})m_{o} \quad (23)$$

Notice that (23) is of the same form as (13) obtained for the case of kriging; however here the known mean m_o enters the equation instead of the BLUE of the unknown mean, $\hat{m}_o$.

By introducing a zero-mean process $Y(x) = Z(x) - EZ(x)$, from (22), the linear-prediction estimator of $Y(x_{\beta})$ is given by

$$Y_{LP}^{*}(x_{\beta}) = \mathbf{C}_{\alpha\beta}^{T}\mathbf{C}_{\alpha\alpha}^{-1}[\mathbf{Z}(x_{\alpha}) - \mathbf{m}_{\alpha}] = \mathbf{C}_{\alpha\beta}^{T}\mathbf{C}_{\alpha\alpha}^{-1}Y(x_{\alpha}) = \boldsymbol{\kappa}_{\beta\alpha}^{T}Y(x_{\alpha}) \quad (24)$$

where $\mathbf{C}_{\alpha\beta} = EY(x_{\alpha})Y(x_{\beta}) = \mathrm{cov}[\mathbf{Z}(x_{\alpha}), Z(x_{\beta})]$; $\mathbf{C}_{\alpha\alpha} = EY(x_{\alpha})Y^{T}(x_{\alpha}) = \mathrm{cov}\,\mathbf{Z}(x_{\alpha})$; and $\boldsymbol{\kappa}_{\alpha\beta}^{T}$ is given by (21). Without loss of generality, it is always possible to consider the zero-mean process $Y(x)$ instead of $Z(x)$. In the following, it is assumed that the linear-prediction estimator of any process can be written as in (24). For the set of estimators at the target points, $[Y_{LP}^{*}(x_{\beta})]^{T} = [Y_{LP}^{*}(x_{n+1}), Y_{LP}^{*}(x_{n+2}), \ldots, Y_{LP}^{*}(x_{n+m})]$, (24) can be written as

$$Y_{LP}^{*}(x_{\beta}) = \mathbf{C}_{\alpha\beta}^{T}\mathbf{C}_{\alpha\alpha}^{-1}Y(x_{\alpha}) \quad (25)$$

CONDITIONAL SIMULATION AND COVARIANCE STRUCTURE

Let $Z^{*}(x_{\beta})$ denote, in general, an unbiased linear estimator, such as the kriging or the linear-prediction estimator, of the spatial random process $Z(x_{\beta})$, expressed by

$$Z^{*}(x_{\beta}) = \boldsymbol{\eta}_{\beta\alpha}^{T}\mathbf{Z}(x_{\alpha}) \quad (26)$$

where $EZ^{*}(x_{\beta}) = EZ(x_{\beta})$. Consider now a simulated process $Z_s(x)$, with known cumulative distribution function, independent of and isomorphic to $Z(x)$ in the sense that the two processes have the same first and second-order statistics. An unbiased linear estimator such as the one in (26) can also be defined for the simulated process $Z_s(x_{\beta})$. The vector of weights $\boldsymbol{\eta}_{\beta\alpha}$ is the same for $Z^{*}(x_{\beta})$ and $Z_s^{*}(x_{\beta})$, since the two processes are isomorphic and provided that the set of recording points, x_{α}, is the same. At any target point x_{β}, the simulated value $Z_s(x_{\beta})$ and the linear estimation based on the corresponding simulated values at the points x_{α} differ by a known amount that can be regarded as a simulated estimation error: $R_s(x_{\beta}) = Z_s(x_{\beta}) - Z_s^{*}(x_{\beta})$. From the unbiasedness of the linear estimator it follows that $ER_s(x_{\beta}) = 0$. The conditional simulation is accomplished by adding the simulated estimation error to the estimator $Z^{*}(x_{\beta})$ as follows (Journel and Huijbregts 1978)

$$Z_{sc}(x_{\beta}) = Z^{*}(x_{\beta}) + [Z_s(x_{\beta}) - Z_s^{*}(x_{\beta})] \quad (27)$$

J. Eng. Mech., 1993, 119(11): 2333-2352

The process $Z_{sc}(x)$ has the same mean as $Z(x)$ due to the lack of bias of $Z^*(x_\beta)$ and the fact that $R_s(x_\beta)$ has zero mean. The requirement of the conditional simulation that observed values be matched at the recording points is satisfied since $Z^*(x_\alpha) = Z(x_\alpha)$ and $[Z_s(x_\alpha) - Z_s^*(x_\alpha)] = 0$, which implies $Z_{sc}(x_\alpha) = Z(x_\alpha)$. To generate $R_s(x_\beta)$, only the joint multivariate density function $f[Z_s(x_\beta), Z_s(x_\alpha)]$ is required to be known. Thus, an advantage of the proposed formulation is that the conditional probability density function $f[Z_s(x_\beta)|Z_s(x_\alpha)]$ does not have to be specified; this function may be difficult to obtain, and its statistics, i.e., the conditional mean and covariance, may be cumbersome functions of the observed values at the recording points. The methodology based on the conditional simulation equation, (27), allows the use of any algorithm that might already be available for the joint multivariate density function $f[Z_s(x_\beta), Z_s(x_\alpha)]$ to generate $[Z_s(x_\beta), Z_s(x_\alpha)]$.

Consider the unknown value of the process at a target point $Z(x_\alpha)$ and its estimator, $Z^*(x_\beta)$, and in particular the conditions under which the unknown estimation error $R(x_\beta) = Z(x_\beta) - Z^*(x_\beta)$ is uncorrelated with the difference $Z^*(x_\gamma) - Z^*(x_\nu)$ between estimated values at two target points (say x_γ and x_ν), or $\text{cov}[Z^*(x_\gamma) - Z^*(x_\nu), R(x_\beta)] = 0$. From (26) the difference between estimated values can be expressed as

$$Z^*(x_\gamma) - Z^*(x_\nu) = \boldsymbol{\eta}_{\gamma\nu}^T \mathbf{Z}(x_\alpha) \quad \ldots\ldots (28)$$

where $\boldsymbol{\eta}_{\gamma\nu} = (\boldsymbol{\eta}_{\gamma\alpha} - \boldsymbol{\eta}_{\nu\alpha})$. Thus

$$\text{cov}[Z^*(x_\gamma) - Z^*(x_\nu), R(x_\beta)] = \boldsymbol{\eta}_{\gamma\nu}^T \text{cov}[\mathbf{Z}(x_\alpha), Z(x_\beta)]$$

$$- \boldsymbol{\eta}_{\gamma\nu}^T \text{cov}\, \mathbf{Z}(x_\alpha)\boldsymbol{\eta}_{\beta\alpha} = \boldsymbol{\eta}_{\gamma\nu}^T(\mathbf{C}_{\alpha\beta} - \mathbf{C}_{\alpha\alpha}\boldsymbol{\eta}_{\beta\alpha}) \quad \ldots\ldots (29)$$

If $\boldsymbol{\eta}_{\beta\alpha} = \mathbf{C}_{\alpha\alpha}^{-1}\mathbf{C}_{\alpha\beta}$, (29) becomes zero and

$$\text{cov}[Z^*(x_\gamma) - Z^*(x_\nu), R(x_\beta)] = 0 \quad \ldots\ldots (30)$$

Therefore, if the estimator in (26) is given by linear prediction, (30) holds. In the case of kriging estimators, we have from (9) that

$$\mathbf{C}_{\alpha\alpha}\boldsymbol{\eta}_{\beta\alpha} = \mathbf{C}_{\alpha\beta} + \frac{1 - \mathbf{J}^T\mathbf{C}_{\alpha\alpha}^{-1}\mathbf{C}_{\alpha\beta}}{\mathbf{J}^T\mathbf{C}_{\alpha\alpha}^{-1}\mathbf{J}}\mathbf{J} \quad \ldots\ldots (31)$$

Substituting (31) into (29), we obtain

$$\text{cov}[Z^*(x_\gamma) - Z^*(x_\nu), R(x_\beta)] = -\frac{1 - \mathbf{J}^T\mathbf{C}_{\alpha\alpha}^{-1}\mathbf{C}_{\alpha\beta}}{\mathbf{J}^T\mathbf{C}_{\alpha\alpha}^{-1}\mathbf{J}}\boldsymbol{\eta}_{\gamma\nu}^T\mathbf{J} \quad \ldots\ldots (32)$$

The term $1 - \mathbf{J}^T\mathbf{C}_{\alpha\alpha}^{-1}\mathbf{C}_{\alpha\beta}$ is zero only when the target point x_β coincides with a recording point. Since this is not the case, the right-hand side of (32) is equal to zero if and only if $\boldsymbol{\eta}_{\gamma\nu}^T\mathbf{J} = 0$, the so-called authorized linear combinations (Journel and Huijbregts 1978). Given that from the unbiasedness condition in (6) we have that $\boldsymbol{\eta}_{\beta\alpha}^T\mathbf{J} = 1$, then

$$\boldsymbol{\eta}_{\gamma\nu}^T\mathbf{J} = \boldsymbol{\eta}_{\gamma\alpha}^T\mathbf{J} - \boldsymbol{\eta}_{\nu\alpha}^T\mathbf{J} = 0 \quad \ldots\ldots (33)$$

Thus for both kriging and linear-prediction estimators, $\text{cov}[Z^*(x_\gamma) - Z^*(x_\nu), R(x_\beta)] = 0$. Using this result it can be shown now that the conditional simulation equation reproduces the variogram of the true process $Z(x)$ when either kriging or linear-prediction estimators are used. The variogram between values at any two target points, x_β and x_ν, denoted here by $2\Delta(x_\beta, x_\nu)$, is equal to

$$2\Delta(x_\beta, x_\nu) = \text{var}[Z(x_\beta) - Z(x_\nu)] = \text{var}[Z^*(x_\beta) + R(x_\beta) - Z^*(x_\nu) - R(x_\nu)]$$

$$= \text{var}[Z^*(x_\beta) - Z^*(x_\nu)] + \text{var}[R(x_\beta) - R(x_\nu)]$$

$$+ 2\text{cov}[Z^*(x_\beta) - Z^*(x_\nu), R(x_\beta) - R(x_\nu)]$$

$$= \text{var}[Z^*(x_\beta) - Z^*(x_\nu)] + \text{var}[R(x_\beta) - R(x_\nu)] \quad \ldots\ldots\ldots\ldots\ldots\ldots (34)$$

where the last equality follows from (30). In the same way the variogram of the conditional simulation can be expressed as

$$2\Delta_{sc}(x_\beta, x_\nu) = \text{var}[Z^*(x_\beta) - Z^*(x_\nu)] + \text{var}[R_s(x_\beta) - R_s(x_\nu)] \quad \ldots\ldots\ldots (35)$$

given that $\text{cov}[Z^*(x_\gamma) - Z^*(x_\nu), R_s(x_\beta)] = 0$, owing to independence between $Z(x)$ and $Z_s(x)$. Since $Z_s(x)$ and $Z(x)$ are isomorphic, then $\text{var}[R(x_\beta) - R(x_\nu)] = \text{var}[R_s(x_\beta) - R_s(x_\nu)]$, and $2\Delta(x_\beta, x_\nu) = 2\Delta_{sc}(x_\beta, x_\nu)$. Therefore, the conditional simulation equation ensures the reproduction of the variogram of $Z(x)$ whether kriging or linear prediction estimators are used.

The covariances for $Z(x)$ and $Z_{sc}(x)$ between values at two target points can be expressed in terms of the variograms as follows.

$$\text{cov}[Z(x_\beta), Z(x_\nu)] = \frac{1}{2}[\text{var } Z(x_\beta) + \text{var } Z(x_\nu)] - \Delta(x_\beta, x_\nu) \quad \ldots\ldots\ldots (36)$$

$$\text{cov}[Z_{sc}(x_\beta), Z_{sc}(x_\nu)] = \frac{1}{2}[\text{var } Z_{sc}(x_\beta) + \text{var } Z_{sc}(x_\nu)] - \Delta_{sc}(x_\beta, x_\nu) \quad \ldots (37)$$

The covariance function of the conditional simulation will be equal to the covariance function of the process $Z(x)$ if $\text{var } Z_{sc}(x_\beta) = \text{var } Z(x_\beta)$, where $\text{var } Z_{sc}(x_\beta)$ is given by

$$\text{var } Z_{sc}(x_\beta) = \text{var } Z^*(x_\beta) + \text{var } Z_s(x_\beta) + \text{var } Z_s^*(x_\beta)$$

$$- 2\text{ cov}[Z_s(x_\beta), Z_s^*(x_\beta)] \quad \ldots\ldots\ldots\ldots\ldots\ldots\ldots\ldots\ldots\ldots\ldots\ldots (38)$$

The terms on the right side of (38) involving $Z^*(x_\beta)$ and $Z_s^*(x_\beta)$ can be obtained from the expression for the linear estimator in (26); thus, $\text{var } Z_s(x_\beta) = C_{\beta\beta}$, $\text{var } Z^*(x_\beta) = \text{var } Z_s^*(x_\beta) = \boldsymbol{\eta}_{\beta\alpha}^T \mathbf{C}_{\alpha\alpha} \boldsymbol{\eta}_{\beta\alpha}$, $\text{cov}[Z_s(x_\beta), Z_s^*(x_\beta)] = \boldsymbol{\eta}_{\beta\alpha}^T \mathbf{C}_{\alpha\beta}$, and

$$\text{var } Z_{sc}(x_\beta) = C_{\beta\beta} + 2\boldsymbol{\eta}_{\beta\alpha}^T(\mathbf{C}_{\alpha\alpha}\boldsymbol{\eta}_{\beta\alpha} - \mathbf{C}_{\alpha\beta}) \quad \ldots\ldots\ldots\ldots\ldots\ldots (39)$$

Since $\boldsymbol{\eta}_{\beta\alpha} \neq 0$, $\text{var } Z_{sc}(x_\beta) = C_{\beta\beta}$ if and only if $\mathbf{C}_{\alpha\alpha}\boldsymbol{\eta}_{\beta\alpha} = \mathbf{C}_{\alpha\beta}$; thus

$$\text{var } Z_{sc}(x_\beta) = C_{\beta\beta} \Leftrightarrow \boldsymbol{\eta}_{\beta\alpha} = \mathbf{C}_{\alpha\alpha}^{-1}\mathbf{C}_{\alpha\beta} \quad \ldots\ldots\ldots\ldots\ldots\ldots\ldots\ldots (40)$$

Therefore, it follows from (40) that the conditional simulation equation reproduces exactly the covariance structure of the true process at any target point when a linear-prediction estimator is used. The use of kriging estimators in the conditional simulation fails to reproduce the covariance structure of the process for any set of target points. Consider as an illustration of a kriging estimator the case in which there is only one recording point x_α, $\alpha = 1$. From (5) and (6), $Z_K^*(x_\beta) = Z(x_1)$, and $Z_s^*(x_\beta) = Z_s(x_1)$. Then, $\text{var } Z_s(x_\beta) = C_{\beta\beta}$, $\text{var } Z_K^*(x_\beta) = \text{var } Z_s^*(x_\beta) = C_{11}$, $\text{cov}[Z_s(x_\beta), Z_s^*(x_\beta)] = \text{cov}[Z_s(x_\beta), Z_s(x_1)] = \rho_{1\beta}\sqrt{C_{\beta\beta}C_{11}}$, where $\rho_{1\beta}$ is the correlation between $Z(x_\beta)$ and $Z(x_1)$. The variance of Z_{sc} is thus

$$\text{var } Z_{sc} = C_{\beta\beta} + 2C_{11} - 2_{\rho 1\beta}\sqrt{C_{\beta\beta}C_{11}} \quad \ldots\ldots\ldots\ldots\ldots\ldots (41)$$

and if $C_{\beta\beta} = C_{11} = \sigma^2$ then

$$\text{var } Z_{sc} = 3\sigma^2 \left(1 - \frac{2}{3}\rho_{1\beta}\right) \quad \ldots\ldots\ldots\ldots\ldots\ldots\ldots\ldots\ldots\ldots\ldots\ldots (42)$$

Eq. (42) shows that when $Z(x_\beta)$ and $Z(x_1)$ are perfectly correlated, $\rho_{1\beta} = 1$, then var $(Z_{sc}) = \sigma^2$. However, as the correlation between them decreases, the variance of the conditional simulation increases, reaching $3\sigma^2$ when there is no correlation at all and $5\sigma^2$ when $\rho_{1\beta} = -1$. Thus, if kriging was used for the conditional simulation of frequency-dependent components of earthquake ground motion, it would be observed that the amplitudes of the motion (and the spectral density) at the target points would become larger as the correlation between motions at target and recording points decreased. An example of a conditional simulation of earthquake ground motion using a kriging estimator is shown in a later section.

CONDITIONAL SIMULATION OF GROUND MOTION

In this section the procedure just described (applicable to frequency-specific ground motion components) is now extended for use in conditional simulation of earthquake ground motion. Consider the simulation of earthquake ground motions at a set of m target points x_β, given that some motions have been recorded at a set of $n = N - m$ recording points, where N is the total number of points. Using (4), the $(N + N)$ covariance matrix $\mathbf{C}_k = [C_{ij}(\omega_k)]$, $i, j = (1, 2, \ldots, n, n + 1, n + 2, \ldots, n + m)$, for each Fourier frequency ω_k, $k = 1, 2, \ldots, (1 + K)/2$, can be assembled and expressed as

$$\mathbf{C}_k = \begin{bmatrix} \mathbf{C}_{\alpha\alpha} & \mathbf{C}_{\alpha\beta} \\ \mathbf{C}_{\alpha\beta}^T & \mathbf{C}_{\beta\beta} \end{bmatrix} \quad \ldots\ldots\ldots\ldots\ldots\ldots\ldots\ldots\ldots\ldots\ldots\ldots (43)$$

Let $\mathbf{A}_s = (\mathbf{A}_{s\alpha}, \mathbf{A}_{s\beta})$ denote a set of simulated Fourier coefficients, where

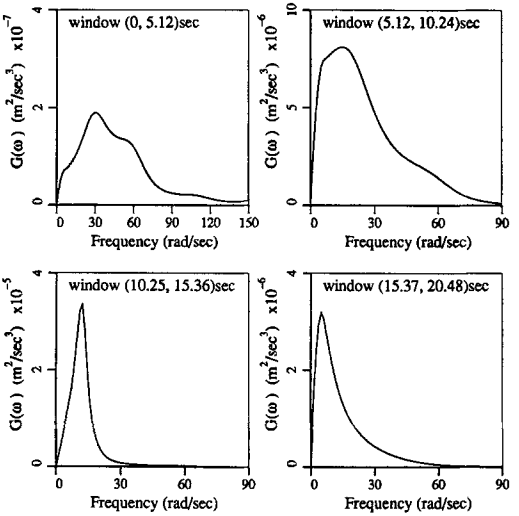

FIG. 1. Power Spectral Density Function for Each Stationary Window

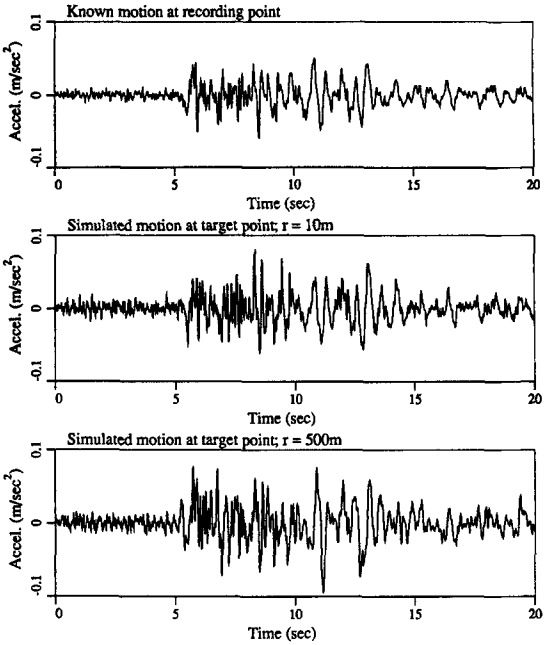

FIG. 2. Conditional Simulations Using Kriging Estimators

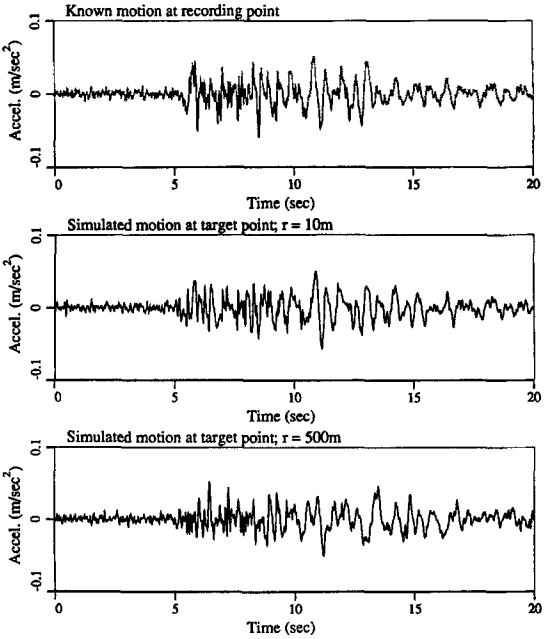

FIG. 3. Conditional Simulations Using Linear-Prediction Estimators

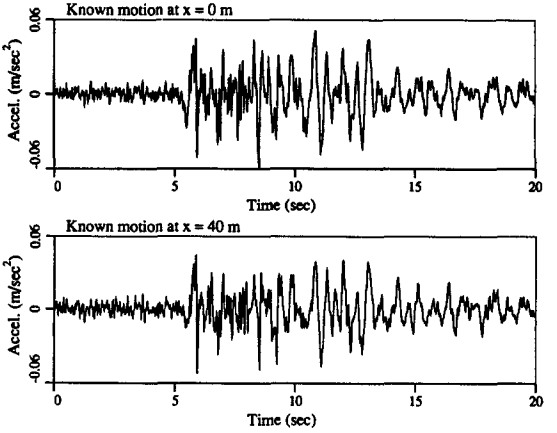

FIG. 4. Prescribed Motions at Recording Points

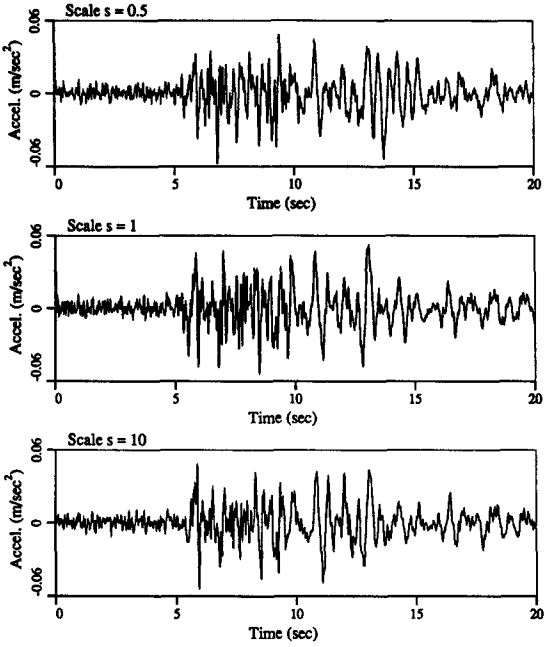

FIG. 5. Conditional Simulations

the subsets $\mathbf{A}_{s\alpha} = (A_{1k}, A_{2k}, \ldots, A_{nk})$ and $\mathbf{A}_{s\beta} = [A_{(n+1)k}, \ldots, A_{(n+m)k}]$ correspond to coefficients at recording and target points, respectively. A set $\mathbf{B}_s$ can be defined similarly. To simulated $\mathbf{A}_s$ and $\mathbf{B}_s$, the covariance matrix $\mathbf{C}_k$ is evaluated for frequencies up to $\omega_{(1+K)/2} = \pi/\Delta t$. For admissible spatial correlation and spectral density functions, C_k is positive definite and can be expressed as the product of a nonsingular lower triangular matrix, $\mathbf{L}_k$, and its transpose by means of a Cholesky decomposition:

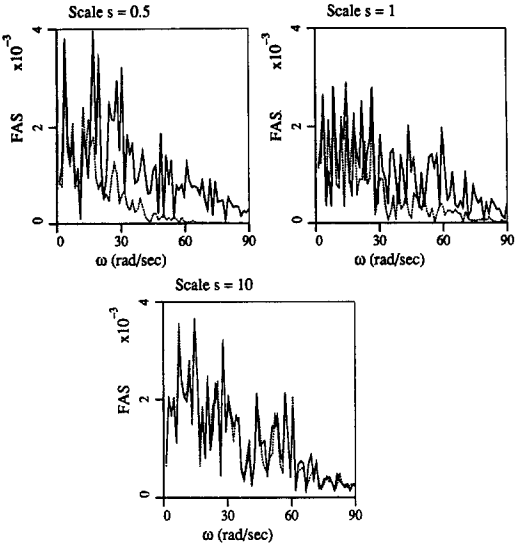

FIG. 6. Fourier Amplitude Spectra for Window (0, 5.12) s

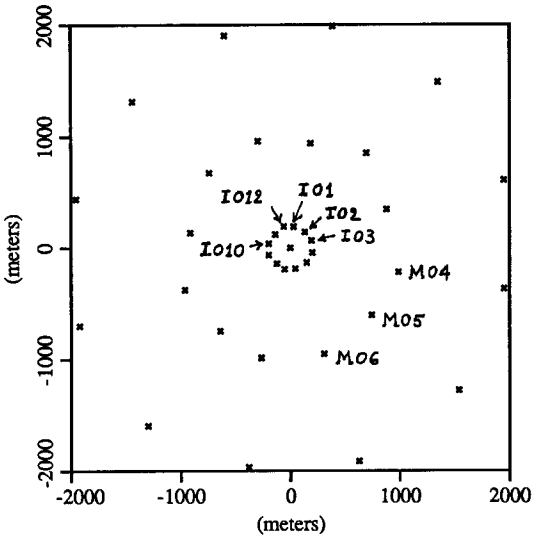

FIG. 7. SMART 1 Array Layout

$$\mathbf{C}_k = \mathbf{L}_k \mathbf{L}_k^T \quad \ldots\ldots (44)$$

In case the limited-duration segment of the ground motion can be modeled as a Gaussian process, we simulate, for each frequency, two sets of independent standard normal random variables, $\mathbf{U}_k = (U_{1k}, U_{2k}, \ldots, U_{Nk})$ and $\mathbf{V}_k = (V_{1k}, V_{2k}, \ldots, V_{Nk})$. The sets $\mathbf{A}_s$ and $\mathbf{B}_s$ are then generated from

$$\mathbf{A}_s = \mathbf{L}_k \mathbf{U}_k \qquad \mathbf{B}_s = \mathbf{L}_k \mathbf{V}_k \quad \ldots\ldots (45)$$

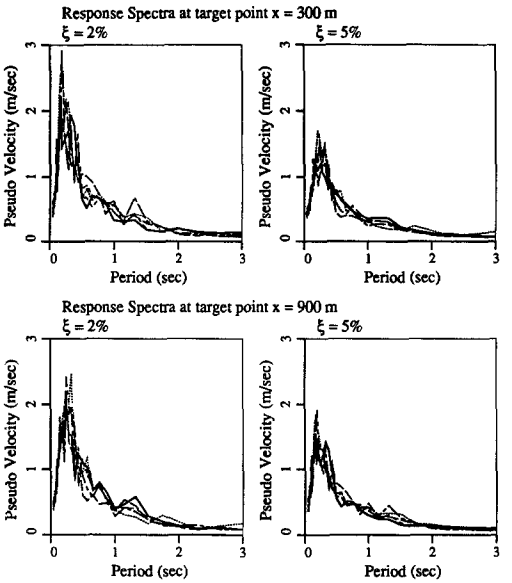

FIG. 8. Response Spectra for 2% and 5% of Critical Damping; Full and Dashed Lines Correspond to Recorded and Simulated Motions, Respectively

One can easily show that $\mathbf{A}_s$ and $\mathbf{B}_s$, have the proper covariance structure. Based on the subsets of simulated values at the recording points, $\mathbf{A}_{s\alpha}$ and $\mathbf{B}_{s\alpha}$, the linear prediction estimators at the target points are given by

$$\mathbf{A}^*_{s\beta} = \mathbf{C}^T_{\alpha\beta}\mathbf{C}^{-1}_{\alpha\alpha}\mathbf{A}_{s\alpha} \qquad \mathbf{B}^*_{s\beta} = \mathbf{C}^T_{\alpha\beta}\mathbf{C}^{-1}_{\alpha\alpha}\mathbf{B}_{s\alpha} \quad \ldots\ldots\ldots\ldots\ldots\ldots\ldots\ldots (46)$$

The conditional simulation now involves generating for each infrequency ω_k, sets of Fourier coefficients $\mathbf{A}_{sc,k} = [A_{(n+1)k}, A_{(n+2)}, \ldots, A_{(n+m)k}]_{sc}$, $\mathbf{B}_{sc,k} = [B_{(n+1)k}, B_{(n+2)k}, \ldots, B_{n+m)k}]_{sc}$, at target points x_β, according to the conditional simulation algorithm in (27), written in vector form as follows.

$$\mathbf{A}_{sc,k} = (\mathbf{A}^*_\beta + A_{s\beta} - \mathbf{A}^*_{s\beta})_{(k)} \qquad \mathbf{B}_{sc,k} = (\mathbf{B}^*_\beta + \mathbf{B}_{s\beta} - \mathbf{B}^*_{s\beta})_{(k)} \quad \ldots\ldots (47)$$

where $\mathbf{A}^*_\beta$ and $\mathbf{B}^*_\beta$ = the linear prediction estimators based on the observed Fourier coefficients at the recording points, $\mathbf{A}_\alpha$ and $\mathbf{B}_\alpha$:

$$\mathbf{A}^*_\beta = \mathbf{C}^T_{\alpha\beta}\mathbf{C}^{-1}_{\alpha\alpha}\mathbf{A}_\alpha \qquad \mathbf{B}^*_\beta = \mathbf{C}^T_{\alpha\beta}\mathbf{C}^{-1}_{\alpha\alpha}\mathbf{B}_\alpha \quad \ldots\ldots\ldots\ldots\ldots\ldots\ldots\ldots (48)$$

The remaining Fourier coefficients at frequencies ω_k, $k = [(2 + k)/2, \ldots, K]$, are then obtained using the symmetry conditions in (3). Once coefficients have been generated for the entire frequency range, an inverse FFT is applied to yield a set of ground motion time histories at the target points.

Summarizing the procedure as presented, the conditional simulation of a limited-duration segment of "aligned" earthquake ground motion consists of the following steps:

1. For each frequency ω_k, $k = 1, 2, \ldots, (1 + K)/2 = \pi/\Delta t$: Obtain from the recorded motions the known Fourier coefficients $\mathbf{A}_\alpha$ and $\mathbf{B}_a$, by means of a direct FFT [(2)]; assemble the covariance matrix $\mathbf{C}_k$ [(43)];

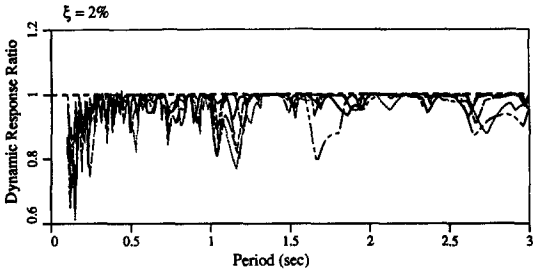

FIG. 9. Dynamic Response Ratio, Span of 30 m; Full and Dashed Lines Correspond to Recorded and Simulated Motions, Respectively

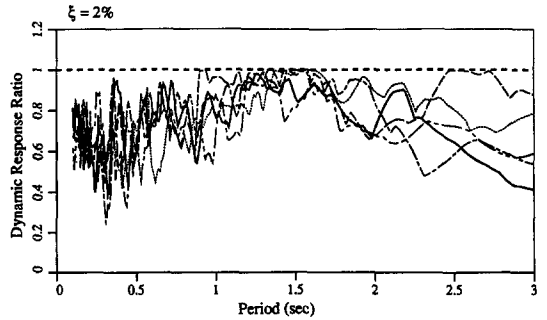

FIG. 10. Dynamic Response Ratio, Span of 300 m; Full and Dashed Lines Correspond to Recorded and Simulated Motions, Respectively

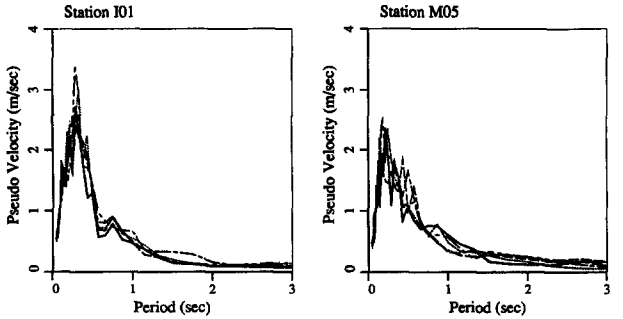

FIG. 11. Response Spectra at Stations I01 and M05, 2% of Critical Damping; Full and Dashed Lines Correspond to Recorded and Simulated Motions, Respectively

simulate at target and recording points the sets of coefficients $\mathbf{A}_s$ and $\mathbf{B}_s$ [(45)]; compute the linear prediction estimators $\mathbf{A}^*_\beta$ and $\mathbf{B}^*_\beta$ based on the known coefficients $\mathbf{A}_\alpha$ and $\mathbf{B}_\alpha$ [(48)]; compute the linear-prediction estimators $\mathbf{A}^*_{s\beta}$ and $\mathbf{B}^*_{s\beta}$ based on the simulations at recording points $\mathbf{A}_{s\alpha}$ and $\mathbf{B}_{s\alpha}$ [(46)]; and generate the conditional simulations $\mathbf{A}_{sc,k}$ and $\mathbf{B}_{sc,k}$ using the algorithm in (47).

2. Generate Fourier coefficients for the entire frequency range using the symmetry conditions in (3).

3. Use an inverse FFT to construct the time-history segments at the target points.

4. To account for nonstationarity, steps 1–3 can be repeated for different input spectral density and frequency-dependent correlation functions to generate stationary segments of ground motion. These segments are then pieced together by means of a linear interpolation algorithm (Vanmarcke and Fenton 1991).

5. The simulated motions may be postprocessed introducing partially predictable wave-propagation phase delays (e.g., Boissieres 1992).

EXAMPLES

In this section some results are presented to illustrate the capabilities and features of the simulation methodology based on linear-prediction theory introduced here. A FORTRAN computer program (SIMQUAKE II) has been written to perform the conditional simulation of earthquake ground motion. The basic inputs to the program are the locations of the points, the spectral density functions (SDFs), the frequency-dependent spatial correlation function, and the known ground motions at the recording points. For the first set of examples, the following isotropic frequency-dependent spatial correlation function has been used.

$$\rho_{\omega k}(\mathbf{r}_{ij}) = \exp\left(\frac{-\omega_k|\mathbf{r}_{ij}|}{2\pi cs}\right) \quad \ldots\ldots\ldots\ldots\ldots\ldots\ldots\ldots\ldots\ldots\ldots\ldots (49)$$

where $\mathbf{r}_{ij}$ = the relative position vector between points x_i and x_j; c = the shear wave velocity in the medium; and s = a distance-scale parameter. The degree of correlation can be controlled by varying s for a fixed distance, or by changing the distance for a fixed value of s. Although the exponential correlation in (49) resembles, within a limited range of separate distances, empirical correlation functions, it is used here solely for illustration purposes. A correlation function estimated from seismic array data is used in later examples.

We first present the results of a comparison between the use of kriging and linear-prediction estimators in conditional simulations for the case of single recording and target points. The recorded ground motion has a sampling frequency of 1/100 s and a total of 2,048 values, and is divided into four successive time windows of 5.12 s each. Maximum entropy estimates of the spectral density function for each window are shown in Fig. 1. The scale parameter s is set at 0.5. Simulations were performed for two interpoint distances $\mathbf{r}$, $\mathbf{r} = |\mathbf{r}_{12}|$, of 10 m and 500 m; those shown in Fig. 2 were obtained using kriging estimators. Since the correlation decays with distance, the amplitudes of the motion tend to grow, indicating an increase in the spectral density and the variance of the ground motion, consistent with the prediction in (42) for the variance of the conditional simulation. The results obtained using linear-prediction estimators are shown in Fig. 3. The motions at both target point locations show a clear difference in the degree of correlation relative to the known motion. As the correlation decreases however there is no increase in the spectral power of the ground motion. Fig. 3 also shows that the use of four stationary-process windows accounts well for the evolution of the frequency content in this case. Each set of simulations in Figs. 2 and 3 took 12 s of computer processing time to run on a VAX machine.

Consider now a conditional simulation where two recording points are at

40 m from each other, and one target point is located halfway between them. Fig. 4 shows the prescribed motions at the recording points. Four stationary time windows of 5.12 s each were selected with spectral density functions as shown in Fig. 1. Fig. 5 presents results for different degrees of correlation implied by values of the scale factor s equal to 0.5, 1, and 10. Fourier amplitude spectra (FAS) obtained from the simulations at the target point are shown in Fig. 6 for one window. The full lines correspond to FAS obtained from the simulated sets of coefficients $\mathbf{A}_{s\beta}$ and $\mathbf{B}_{s\beta}$, whereas the dashed lines correspond to the FAS using the linear-prediction estimators $\mathbf{A}^*_{s\beta}$ and $\mathbf{B}^*_{s\beta}$. For low degrees of correlation, $s = 0.5$, the main contribution to the conditional simulation comes from the simulated coefficients $\mathbf{A}_{s\beta}/\mathbf{B}_{s\beta}$. In the extreme case of no correlation, knowing the recorded motions should have no effect on the simulation at the target points, the conditional simulation being determined solely by the simulated Fourier coefficients, $\mathbf{A}_{s\beta}$ and $\mathbf{B}_{s\beta}$. As the correlation increases, the contribution from the linear prediction estimates becomes larger, as shown in Fig. 6, and should eventually match the simulated $\mathbf{A}_{s\beta}$ and $\mathbf{B}_{s\beta}$ for the case of perfect correlation. In this case, the conditional simulation can be obtained from the recorded Fourier coefficients $\mathbf{A}_\alpha$ and $\mathbf{B}_\alpha$.

Conditional simulations have also been performed using data recorded by the SMART 1 array (Abrahamson et al. 1987) during the event of December 17, 1982 ($M_L = 6.4$, $\Delta = 79KM$, azimuth of 99°). The array, located in Lotung, Taiwan, consists of 37 stations deployed in three concentric rings of radii 200 m, 1,000 m and 2,000 m (see Fig. 7). Based on analysis of recorded data, Harichandran and Vanmarcke (1986) proposed the following model for the frequency-dependent spatial correlation function of phase-aligned ground accelerations:

$$\rho_{\omega k}(\mathbf{r}_{ij}) = 0.736 \exp\left(\frac{-5.063|\mathbf{r}_{ij}|}{\theta_\omega}\right) + 0.294 \exp\left(\frac{-0.744|\mathbf{r}_{ij}|}{\theta_\omega}\right) \quad \ldots\ldots (50)$$

where

$$\theta_\omega = 5{,}210\left[1 + \left(\frac{\omega}{2.18\pi}\right)^{2.78}\right]^{-1/2} \quad \ldots\ldots\ldots\ldots\ldots\ldots\ldots\ldots (51)$$

is the frequency-dependent scale of fluctuation (Vanmarcke 1983).

This model for the correlation function has been used in all the examples that follow. The first results correspond to a five-point conditional simulation where three recording points are located on a straight line and two target points are midway in between them. The distance between consecutive points, or the span, is constant and equal to 300 m. Assumed known ground motions at all five points were generated first by running the program once for the case of five target points. Then the simulated motions at the locations of the recording points were taken as the input known motions for the conditional simulations. The simulated motions at the target points were used as the known ground motions for comparison with the output from the conditional simulations. A time step of 0.01 s was used and two windows of 5.12 s each were considered. Fig. 8 shows response spectra plots for 2% and 5% of critical damping; note that the spectra from the simulated motions agree well with those from the known motions. The point variance of the ground motion was obtained by integrating the input SDF, and estimated variances over an ensemble of realizations were within 5% of the specified input variance.

For both types of comparisons used—the response spectrum and the point variances—ground motions are taken one at a time and analyzed independently of the other motions, thus neglecting the actual spatial patterns. To verify that the algorithm is producing properly correlated motions in space we used the dynamic response ratio (DRR) developed by Loh et al. (1982), and later expanded by Abrahamson and Bolt (1985), for studying the seismic response of multiply supported structures. To obtain the DRR it is assumed that the normal modes of the structure are known and that for each mode, the participation factors corresponding to each input support displacement are also known. They all depend on the mass and stiffness properties of the structure. For each mode, and for each unconstrained degree of freedom of the structure, the DRR is defined as the ratio of the maximum response of the structure due to the ground accelerations at the supports, to the average of the maximum response obtained using each individual support acceleration as a rigid base input. Consider the case of a single-degree-of-freedom shear building model consisting of a rigid mass and two columns supported at points A and B. The fundamental mode of the system is excited by the "in-phase" motion and the DRR is given by

$$\Phi^d(\xi, T) = \frac{S_a^{AB}(\xi, T)}{S_a^{AA}(\xi, T) + S_a^{BB}(\xi, T)} \quad \ldots\ldots\ldots\ldots\ldots\ldots\ldots\ldots (52)$$

where $S_a^{AB}(\xi, T)$ = the standard pseudo-acceleration response spectrum for an input motion equal to the sum of ground accelerations at supports A and B; $S_a^{AA}(\xi, T)$ and $S_a^{BB}(\xi, T)$ = the standard pseudo acceleration response spectra for the ground accelerations at supports A and B, respectively; ξ = the damping coefficient; and T = the natural period.

Figs. 9 and 10 show plots of DRR versus period for 2% damping for spans of 30 m and 300 m. The known and simulated ground motions were taken as the support motions. The full lines correspond to the DRR obtained from the known motion, and the dashed lines to ratios computed using the simulations. For the 30-m span, the DRR is virtually equal to 1.0 for most of the period range, implying a high degree of correlation between motions. The DRR computed from the simulated and known motions follow the same trend. In the case of the 300-m span, the DRR shows a trend toward one as period increases in the range of 1–1.5 s, and then decreases for the longer periods, indicating a lower degree of correlation compared to the 30-m case. Again, it is seen here that the DRR obtained from the known and simulated motions tend to follow the same trend quite closely.

Now consider a test of the simulation against reality, based on ground motions recorded by the SMART 1 array. Stations I01, I03, and I10 in the inner ring were taken as the recording points and motions in the epicentral direction were simulated at stations I02 and I12 (target points). The time step of the known ground motions is 0.01 s and two windows of 512 time steps were considered. For each window the spectral density functions were taken as the average of the estimated SDF from the known ground motions. A six-point simulation was performed to test the ability of the methodology to produce properly correlated ground motions at larger distances. In this case, the stations I12 and I02 in the inner ring and M04 and M06 in the middle ring were taken as the recording points. The target points were assumed to be the stations I01 and M05, located 1,070 m from each other. Several simulations were performed in the epicentral direction using two stationary segments of 5.12 s each. For each window the spectral density function was modeled by the average of the estimated SDF from the four

known ground motions. Fig. 11 shows the plots of response spectra for 2% of critical damping, for the recorded motions and four simulations. Note that the simulations lead to response spectra that are in very good agreement with those obtained from the recorded motions. The DRR for the simulated motions also follows the same trend as that for the known motions.

CONCLUSIONS

Improved methodology has been developed for conditional simulation of earthquake ground motion. Recorded motions may be known or specified for seismic design and analysis purposes at some surface points, and compatible ground motions are to be generated at locations where they are not known. The simulation technique developed here is based on the theory of multivariate linear prediction, and ensures the unbiased reproduction of the covariance structure of the ground motion; in this respect, it is a significant improvement over existing kriging techniques. Also, the simulation is accomplished by superposing statistically independent frequency-specific spatial field whose component variances and correlation distances are obtained, respectively, from the ground motion spectral density function and frequency-dependent spatial correlation function.

A computer program (SIMQUAKE II) has been written for the conditional simulation of fields of earthquake ground motion; it uses FFT techniques which make the computations highly efficient. The input to the program consists of the location of the field points, the prescribed known motions, and the covariance structure expressed by the frequency-dependent spatial correlation and the point spectral density functions. Several examples have been presented to illustrate the features of the methodology. Response spectra, spectral density function, and dynamic-response ratios have been used to compare simulated and recorded ground motions, and the results indicate on the whole very good agreement. The methodology can easily be extended to the simulation of non-homogeneous earthquake ground motion, allowing incorporation of varying local site conditions through location-dependent spectral density functions.

ACKNOWLEDGMENTS

We thank G. Watson for helpful comments and stimulating discussions on the topic of conditional simulation. This research was performed as part of a project entitled "2D and 3D Ground Motion Studies," supported by the National Science Foundation through National Center for Earthquake Engineering Research Contract 91-2031B. Any opinions, findings, conclusions, or recommendations are those of the writers and do not necessarily reflect the views of the sponsors.

APPENDIX I. REFERENCES

Abrahamson, N., and Bolt, B. (1985). "The spatial variation of the phasing of seismic strong ground motion." *BSSA*, 75(5), 1247–1264.

Abrahamson, N., et al. (1987). "The SMART 1 accelerograph array (1980–1987): A review." *Earthquake Spectra*, 3(2), 267–287.

Boissieres, H. P. (1992). "Estimation of the correlation structure of random fields," PhD thesis, Princeton University, Princeton, N.J.

Harichandran, R., and Vanmarcke, E. (1986). "Stochastic variation of earthquake ground motion in space and time." *J. Engrg. Mech.*, ASCE, 112(2), 154–174.

Heredia-Zavoni, E. (1993). "Structural response to spatially varying earthquake

ground motion," PhD dissertation, Princeton University, Princeton, N.J.
Journel, A., and Huijbregts, C. H. (1978). *Mining geostatistics*. Academic Press, London, England.
Loh, C., Penzien, J., and Tsai, Y. (1982). "Engineering analysis of SMART 1 array accelerograms." *Earthquake Engrg. Struct. Dyn.*, 10(2), 575–591.
Matheron, G. (1967). "Kriging or polynomial interpolation procedures." *Can. Inst. of Mining Bull.*, 60(4), 1041–1053.
Priestley, M. B. (1981). *Spectral analysis and time series*, Academic Press, New York, N.Y.
Vanmarcke, E. (1983). *Random fields: analysis and synthesis*. The MIT Press, Cambridge, Mass.
Vanmarcke, E., and Fenton, G. (1989). "Application of kriging techniques to earthquake ground motion simulation." *Proc. 4th Int. Conf. on Soil Dyn. and Earthquake Engrg.*, A. Cakmak and I. Herrera, eds., Computational Mechanics, 247–263.
Vanmarcke, E., and Fenton, G. (1991). "Conditioned simulation of local fields of earthquake ground motion." *Struct. Safety*, 10(1–3), 247–264.
Watson, G. S. (1970). "Trend surface analysis." *Technical Report No. 143*, Dept. of Statistics, John Hopkins Univ., Baltimore, Md.

APPENDIX II. NOTATION

The following symbols are used in this paper:

A_{ik}, B_{ik} = Fourier coefficients at point x_i for frequency ω_k;
$\mathbf{A}_s$, $\mathbf{B}_s$ = sets of simulated Fourier coefficients;
$\mathbf{A}_{sc,k}$, $\mathbf{B}_{sc,k}$ = sets of conditional simulations of Fourier coefficients;
$\mathbf{A}_\alpha$, $\mathbf{B}_\alpha$ = sets of known Fourier coefficients;
$\mathbf{A}^*_\beta$, $\mathbf{B}^*_\beta$ = sets of linear-prediction estimators based on $\mathbf{A}_\alpha$ and $\mathbf{B}_\alpha$;
$\mathbf{A}^*_{s\beta}$, $\mathbf{B}^*_{s\beta}$ = sets of linear-prediction estimators based on $\mathbf{A}_s$ and $\mathbf{B}_s$;
$C_{ij}(\omega_k)$ = covariance of A_{ik} and A_{jk};
$\mathbf{C}_k$ = covariance matrix for Fourier coefficients at frequency ω_k;
$\mathbf{C}_{\alpha\beta}$, $\text{cov}[\mathbf{Z}(x_\alpha), Z(x_\beta)]$ = covariance matrix of $\mathbf{Z}(x_\alpha)$ and $Z(x_\beta)$;
$\mathbf{C}_{\alpha\alpha}$, $\text{cov}\mathbf{Z}(x_\alpha)$ = covariance matrix of $\mathbf{Z}(x_\alpha)$;
$EZ(x)$ = expected value of $Z(x)$;
$f[Z_s(x_\beta), Z_s(x_\alpha)]$ = joint multivariate probability density function of $Z_s(x_\beta)$ and $Z_s(x_\alpha)$;
$G(\omega)$ = one-sided point spectral density function;
$\mathbf{J}$ = n-dimensional vector of ones;
L_k = lower triangular matrix from Cholesky decomposition of $\mathbf{C}_k$;
n = number of recording points;
m = number of target points;
m_o = constant mean;
$\hat{m}_o$ = best linear unbiased estimator (BLUE) of m_o;
$\mathbf{m}_\alpha$ = mean of $\mathbf{Z}(x_\alpha)$;
m_β = mean of $Z(x_\beta)$;
$\mathbf{r}_{ij}$ = relative position vector;
$R(x_\beta)$ = unknown estimator error;
$R_s(x_\beta)$ = simulated estimator error;

$\mathrm{Re}(\ )$ = real part of argument;
$S_a(\xi, T)$ = standard pseudo-acceleration response spectrum;
$S_a^I(\xi, T)$ = standard pseudo-acceleration response spectrum for input $\mathbf{I}$;
s = distance-scale parameter in $\rho_{wk}(\mathbf{r}_{ij})$;
T = natural period;
t, t_f = time;
$\mathrm{var}Z(x)$ = variance of $Z(x)$;
x, x_i, x_j = point in space;
x_α = recording point;
x_β, x_γ, x_ν = target point;
$Y(x)$ = zero-mean spatial random process;
$Z(x)$ = spatial random process;
$Z(x_\beta)$ = unknown value of $Z(x)$;
$\mathbf{Z}(x_\alpha)$ = set of known values of $Z(x)$;
$Z^*(x_\beta)$ = general unbiased linear estimator of $Z(x)$;
$Z_i,(t)$ = space time random process;
$Z_K^*(x_\beta)$ = kriging estimator of $Z(x)$'
$Z_{LP}^*(x_\beta)$ = linear-prediction estimator of $Z(x)$;
$Z_s(x)$ = simulated random process;
$Z_{sc}(x)$ = conditional simulation of $Z(x)$;
U_k, V_k = sets of independent standard normal random variables;
$\Delta(x_\beta, x_\gamma)$ = variogram of $Z(x_\beta)\ Z(x_\gamma)$;
$\Delta t, \Delta w$ = time and frequency steps;
$\boldsymbol{\kappa}_{\beta\alpha}$ = vector of linear-prediction coefficients;
$\boldsymbol{\lambda}_{\beta\alpha}$ = vector of kriging weights;
$\boldsymbol{\eta}_{\beta\alpha}^T$ = vector of weights for $Z^*(x_\beta)$;
ξ = damping coefficient;
$\Phi^d(\xi, T)$ = dynamic response ratio;
$\rho_{wk}(\mathbf{r}_{ij})$ = frequency-dependent spatial correlation function;
σ^2 = variance of homogeneous process;
θ_ω = frequency-dependent scale of fluctuation; and
ω, ω_k = frequency (rad/s).